Geophysical Research Letters

RESEARCH LETTER
10.1029/2022GL102146

Monitoring Seasonal Fluctuation and Long-Term Trends for the Greenland Ice Sheet Using Seismic Noise Auto-Correlations

Bingxu Luo[1], Shuo Zhang[1], and Hejun Zhu[1,2]

[1]Department of Geosciences, The University of Texas at Dallas, Richardson, TX, USA, [2]Department of Physics, The University of Texas at Dallas, Richardson, TX, USA

Key Points:

- The seasonal variations of relative velocity change (*dv/v*) have <3 months lag with respect to the surface Greenland Ice Sheet (GrIS) change
- Larger lag times of *dv/v* may provide constrains for thicker subglacial till layers in the central Greenland
- *dv/v* may be used for monitoring long-term GrIS mass change

Supporting Information:

Supporting Information may be found in the online version of this article.

Correspondence to:

H. Zhu,
hejun.zhu@utdallas.edu

Citation:

Luo, B., Zhang, S., & Zhu, H. (2023). Monitoring seasonal fluctuation and long-term trends for the Greenland Ice Sheet using seismic noise auto-correlations. *Geophysical Research Letters*, *50*, e2022GL102146. https://doi.org/10.1029/2022GL102146

Received 14 NOV 2022
Accepted 28 FEB 2023

Abstract One important feature of the Greenland Ice Sheet (GrIS) change is its strong seasonal fluctuation. Taking advantage of deployed seismographic stations in Greenland, we apply cross-component auto-correlation of seismic ambient noise to measure in-situ near surface relative velocity change (*dv/v*) in different regions of Greenland. Our results demonstrate that *dv/v* measurements for most stations have less than 3 months lag times in comparison to the surface mass change. These various lag times may provide us constraints for the thickness of the subglacial till layer over different regions in Greenland. Moreover, in southwest Greenland, we observe a change in the long-term trend of *dv/v* for three stations, which might be consistent with the mass change rate (*dM/dt*) due to the "2012–2013 warm-cold transition." These observations suggest that seismic noise auto-correlation technique may be used to monitor both seasonal and long-term changes of the GrIS.

Plain Language Summary The changes of the Greenland Ice Sheet (GrIS) have important implications for both scientific research and human society. Due to its large size, the change of the GrIS varies at different regions. Here, we apply a seismic monitoring technique to study the GrIS mass change by using seismographic stations deployed in Greenland. The advantage of using this technique is that we are able to monitor different locations in a relatively simple, low-cost and in-situ way, and obtain indicative information about the ice mass change over time. We specify the seasonal fluctuations of seismic signals and connect them with the subglacial setting at different regions in Greenland, and explore the potential of using these seismic techniques to monitor the long-term changes of the GrIS.

1. Introduction

The Greenland Ice Sheet (GrIS), the second largest ice body in the world (after the Antarctic ice sheet), stores ~3 million km^3 worth of ice (Programme for Monitoring of the Greenland Ice Sheet, 2022) (PROMICE webpage: https://promice.org/greenland-ice-sheet). Over the past several decades, the GrIS encounters increasing mass loss due to local warming, and has become the major contributor to the global sea-level rise (Morlighem et al., 2017; Shepherd et al., 2012; The IMBIE Team, 2020; Trusel et al., 2018; Zheng et al., 2022). To date, the GrIS still holds enough water to potentially raise the mean sea-level over 7.4 m (Morlighem et al., 2017). One important feature of the mass change of the GrIS is that it has strong seasonal fluctuation (one-year cycle). The overall seasonal mass loss/gain is mainly due to large meltwater runoffs in the summertime, and overall high precipitation in the wintertime (Joughin et al., 2008; Mordret et al., 2016; Mouginot et al., 2019; Rignot et al., 2008). Besides this seasonal fluctuation, there is a specific long-term trend of the GrIS in recent decades. For instance, an abnormal warm-cold transition during 2012–2013 has been noted in many studies (Bevis et al., 2019; Harig & Simons, 2016; Khazendar et al., 2019; The IMBIE Team, 2020). This transition results in 222 Gt (1 Gt = 10^{12} kg) annual mass loss of the GrIS during 2013–2017, which is around 35% reduction of its peaking level (345 Gt) in 2011–2012 (The IMBIE Team, 2020).

One common method for monitoring the global ice sheets change is using satellite or/and radar altimetry to measure the ice sheet volume (Helm et al., 2014; Pritchard et al., 2009; Sandberg Sørensen et al., 2018; Zwally et al., 2005). However, current radar systems do not perform well when the ice sheet change is rapid, because of inaccurate assumptions on the density profiles of firn compaction (Machguth et al., 2016; Pritchard et al., 2009). Detecting gravitational anomalies of the ice sheet mass change also has been widely used since the launch of the Gravity Recovery and Climate Experiment (GRACE) mission in March 2002 (http://www2.csr.utexas.edu/grace/). Many studies have used the GRACE data to estimate the GrIS mass change, which show strong seasonal

fluctuation and continuous mass loss over the past two decades (Bevis et al., 2019; Chen et al., 2006; Harig & Simons, 2016; Luthcke et al., 2006; Ramillien et al., 2006). However, the GRACE data has limited spatial (~300 km in Greenland) and temporal (one-month) resolutions. Other methods include using Global Positioning System (GPS) to track ice movement and crustal uplifting (Bevis et al., 2019; Harig & Simons, 2012; Khan et al., 2014), and building input-output flux models through mass budget methods (Mouginot et al., 2019; Velicogna et al., 2020).

Over the past decades, seismologists have used continuous ambient noise recorded by a pair of seismic sensors to retrieve temporal changes in phase delay times, which are then used to measure near surface velocity changes between two locations (Campillo & Paul, 2003; Lecocq et al., 2014). This technique takes advantage of continuous recording from seismic stations, and was initially applied to monitor changes associated with volcanic edifices and fault zones (Brenguier et al., 2008; Mordret et al., 2010; Sens-Schönfelder & Wegler, 2006; Wegler & Sens-Schönfelder, 2007). Recently, it has been used to estimate relative seismic velocity changes (dv/v) in Greenland. For instance, Mordret et al. (2016) study 2-year seismic records from station pairs deployed in southwest/west Greenland, demonstrating strong seasonal fluctuation in dv/v measurements. They propose a poroelastic model to explain these observations, which may result from surface ice mass loading/unloading and induced strains within the crust. Later, Toyokuni et al. (2018) utilize 4.5-year seismic records from station pairs in different parts of Greenland to monitor both long term trends and seasonal fluctuation of dv/v in different regions of Greenland. However, the cross-correlation measurements from station pairs are typically affected by their low singal-to-noise ratio due to energy scattering through long interdistances between stations, which is critical in Greenland due to its sparse station coverage. Thus, in this study, we collect 11 seismographic stations from different regions of Greenland, and retrieve dv/v by using cross-component auto-correlation of seismic ambient noise. We attempt to study both long term trend (including the "2012–2013 transition") and seasonal fluctuation for different parts of Greenland over the past two decades.

2. Data and Methods

2.1. Continuous Seismic Records

We perform cross-component (north-south and west-east components) auto-correlation for each individual station, except for two stations ANGG and ISOG, which are calculated by using cross-correlation due to their short separation (~50 km). The advantages of using this auto-correlation technique include: (a) we can specify local dv/v at individual station, instead of a wide sampling region between stations. Since the mass change of the GrIS may have strong spatial variations (Bevis et al., 2019; Mouginot et al., 2019; The IMBIE Team, 2020); (b) we can retrieve correlation functions with high signal to noise ratio, because the seismic phases we measure do not travel long distances between stations. Here, we collect broadband (with the sampling rate of 20 Hz) seismic data for nine stations in Greenland, and long period (with the sampling of 1 Hz) data for stations ILULI and DY2G due to their limited bandwidth. We collect data for all stations with availability ranging from 7 to 21 years (more information for seismic stations can be found in Table S1 in Supporting Information S1).

2.2. Seismic Data Processing and dv/v Measurements

We use the MSNoise package (Lecocq et al., 2014) to perform noise correlation and measure dv/v. All seismic records are demeaned, detrended and filtered from 0.1 to 1 Hz, except applying 0.1–0.5 Hz bandpass filter for stations ILULI and DY2G due to their limited bandwidth. The next step is to compute auto-correlation functions (ACFs) between two horizontal components. We set the analysis duration as 86,400 s (one day) and cut each daily trace into 1,800 s slices (with a 50% overlap) to perform correlation, which gives us all daily ACFs. We set three times root mean squares (RMS) as extreme limits to suppress outliers (e.g., local seismicity) and a spectral whitening for each correlation slice (1,800 s) is used. The final step is to use the moving-window cross spectrum (MWCS) technique to measure dv/v (Clarke et al., 2011), which estimates the relative time delay (dt/t) between current and reference ACFs in the frequency domain. We set the minimum cross coherence value as 0.75, and measure dv/v by using data in the ACFs above this level, so that we can mitigate temporal variability due to inhomogeneous source distributions. If we assume the change of dv/v is spatially homogeneous, then

$$dv/v = -dt/t, \tag{1}$$

We can directly retrieve *dt/t* by using a weighted linear regression (see more details in Text S1 in Supporting Information S1). Figure S1 in Supporting Information S1 shows an example of seismic noise correlation and *dv/v* measurement for station NRS. To make a balance between mitigating recording gaps and keeping high temporal resolutions, we test different moving-window stacks for ACFs (with 90, 120, and 150 days in Figures S1c–S1e in Supporting Information S1), and finally choose 150 days stacking for the following analysis. The MWCS filter and other control parameters are listed in Table S2 in Supporting Information S1 and shown in Figure S1b in Supporting Information S1.

To test different frequency response for the *dv/v* measurements, we first perform a short-time Fourier transform to analyze their time-frequency features. We observe that the strongest signal ranges from 0.1 to 0.4 Hz (Figure S2 in Supporting Information S1). Then we measure *dv/v* using different frequency ranges (Figure S3 in Supporting Information S1). Larger *dv/v* amplitudes and higher noise levels can be observed in the lower frequency band (0.1–0.5 Hz), and weaker seasonal fluctuation and long-term trend are observed in the higher frequency band (1–2 Hz). Therefore, we choose 0.1–1 Hz for our following discussions. Furthermore, the selection of measurement windows inside the ACFs is quite important for analyzing and interpreting *dv/v* measurements (Lecocq et al., 2014). Here, we apply different windows (*dt*, time delays) from early to late coda arrivals to test the variability of *dv/v* measurements. We test three different windows (Figure S4a in Supporting Information S1) on four selected stations, the measured *dv/v* from testing windows present highly consistent seasonal variation (top panels in Figures S4b–S4e in Supporting Information S1) with our current window (20–70 s). This consistency between different windows suggest that our *dv/v* measurements mainly reflect subsurface velocity changes, instead of changes from ambient noise source distributions. However, we do not exclude that the most direct (from 0 s) or very late coda (>80 s) portions may bring additional biases to our *dv/v* measurements. Thus, it is safe to select 20–70 s window portion to achieve robust *dv/v* measurements for the following analysis. In addition, we also compute auto-correlation sensitivity kernels based on assumptions from Pacheco and Snieder (2005) (More details can be found in Text S2 in Supporting Information S1). This auto-correlation kernel can be described as energy diffusion approximation of multiple scattering wave fields, which only depend on time delays (windows) and location in homogeneous media (Pacheco & Snieder, 2005; Richter et al., 2014). In Figure S5 in Supporting Information S1, the results suggest that our selected window portion (20–70 s) is more sensitive to velocity perturbations at depths shallower than 4 km.

3. Results

3.1. Correlations Between *dv/v* and Surface Ice Mass Change

The total GrIS mass balance (TotalMB) mainly includes surface ice mass balance (SMB) and ice discharge (D). The SMB is balanced by the accumulation and runoffs of the surface ice sheet, while D represents ice discharge and calving at the ice-ocean boundaries. Thus, TotalMB = SMB - D (Bevis et al., 2019; Mouginot et al., 2019). Here, we use a data set that separately reconstructs SMB and D by using regional climate models provided by the Program for Monitoring of the Greenland Ice Sheet, Denmark (Mankoff et al., 2021). This data set provides results for seven drainage basins (south-west: SW; south-east: SE; central-west: CW; central-east: CE; north-west: NW; north-east: NE; north: NO) in Greenland (Mouginot & Rignot, 2019). For both regional and total GrIS, the seasonal fluctuation of TotalMB is dominated by SMB, while D has very weak seasonal fluctuation even though with large portions in some regions (Figure S6 in Supporting Information S1).

In Figure 1, we observe similar seasonal fluctuation of *dv/v* for most stations that follows the variation of regional SMB. Here, we perform cross-wavelet transform between *dv/v* for regional SMB and each individual station, so that we can analyze their time-frequency features as well as the lag times between these two time series (Mao et al., 2019; Torrence & Compo, 1998). Moreover, we use coefficient of variation (CV, the ratio of standard deviation to mean value) to quantify the variability of measured lag time. A smaller CV value suggests a lag time with smaller temporal variability. For example, in the bottom panel of Figure 1c, the strongest signal suggests that the *dv/v* for station SFJD has a clear one-year cycle, and an averaged lag time of 67 days with respect to the SMB in the SW region. More details about wavelet transform analysis can be found in Text S3 in Supporting Information S1.

Five stations (ILULI, SFJD, DY2G, NUUK, and NRS) in the SW/CW Greenland have averaged lag times of 34, 67, 84, −38, and 35 days with respect to the regional SMB, respectively (Figures 1b–1f). In the NE and CE Greenland, both stations DAG and SCO have the same averaged lag time of 64 days with respect to the regional SMB (Figures 1g and 1h). In addition, in the SE Greenland, the *dv/v* for station pair ANGG-ISOG has an averaged lag time of 55 days with respect to the SMB (Figure 1i). Table 1 summarizes the lag times between *dv/v* and regional SMB (with CV values) for these stations in Greenland.

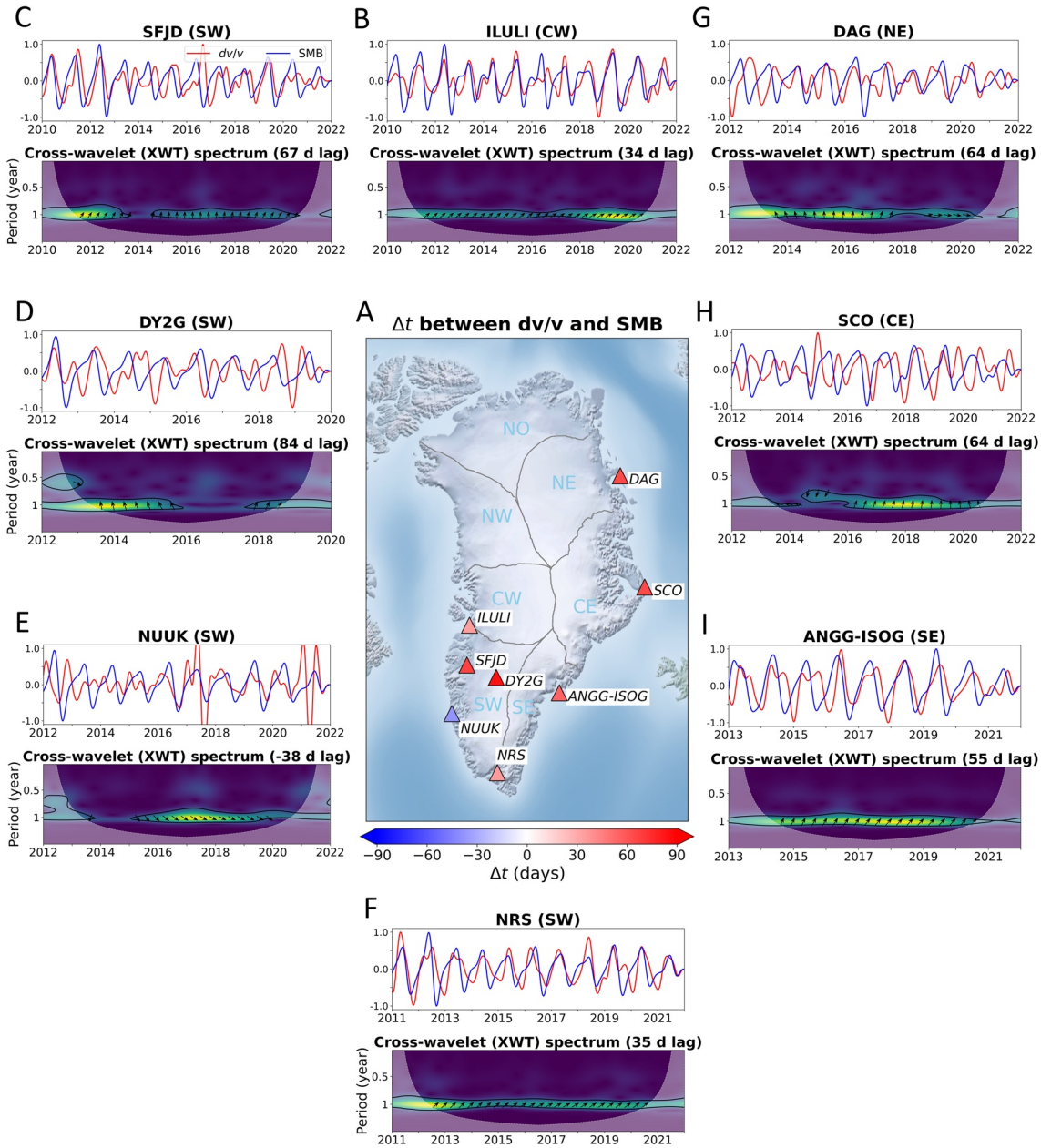

Figure 1. Correlations between *dv/v* with surface mass change (SMB) for different regions of Greenland. Panel (a) shows seismic stations (triangles) in seven drainage basins (Mouginot & Rignot, 2019). In Panels (b–i), top panel: *dv/v* (red) and regional SMB (blue) time series, both of them are detrended, normalized and filtered in 8- to 36-month period; bottom panel: cross-wavelet transform between these two datasets. The white shade represents the influential cone due to edge effects, the black contour represents 99% confidence level against red noise. Arrows denote local phase angles, we set 0°to right. All amplitude spectra are normalized. The average lag times (Δt) are labeled in Panels (b–i) and color-coded in Panel (a).

3.2. Correlations Between *dv/v* and Snowfall Rate

The seasonal fluctuation of the GrIS is mainly due to melting water runoffs in the summertime, and higher precipitation and refreezing in the wintertime (Joughin et al., 2008; Mordret et al., 2016; Mouginot et al., 2019; Rignot et al., 2008). However, this process may not work for the central Greenland, which has much lower temperature during the summertime because of its higher altitude (Figure S7 in Supporting Information S1). Stations SUMG and ICESG are located in the central Greenland, which cannot be included in any one of the seven drainage basins. Therefore, we perform the cross-wavelet transform between *dv/v* with local snowfall rates for these two stations, since the snowfall probably dominates the surface mass change in the central Greenland

Table 1
Averaged Lag Times (Δt) Between dv/v and Surface Mass Change (SMB) or Snowfall Rates for Different Stations

Stations	Reference	Δt (days)	Coefficient of variation	Region
ILULI	SMB	34	0.23	CW
SFJD	SMB	67	0.28	SW
NRS	SMB	35	0.17	SW
DY2G	SMB	84	0.53	SW
DAG	SMB	64	0.73	NE
SCO	SMB	64	1.31	CE
ANGG-ISOG	SMB	55	0.16	SE
SUMG	Snowfall	−59	1.54	Central
ICESG	Snowfall	82	0.14	Central
NUUK	Snowfall	44	0.67	SW

(Toyokuni et al., 2018). We use the snowfall rate data set from ERA5 (https://www.ecmwf.int/en/forecasts/datasets/reanalysis-datasets/era5), which is the fifth generation global climate and weather data set provided by the European Centre for Medium-Range Weather Forecasts (Hersbach et al., 2018). Moreover, we note that the *dv/v* for station NUUK does not have a positive correlation with the SMB (Figure 1e). Thus, we also try to correlate *dv/v* with the local snowfall rate for station NUUK.

In the central Greenland, the *dv/v* of stations SUMG and ICESG have averaged lag times of −59 and 82 days with respect to their local snowfall rates (Figures 2b and 2d). The *dv/v* for station SUMG has responses when there are extreme changes in the snowfall rates, such as 2015–2019, even though its poor seasonal fluctuation (Figure 2b). Station NUUK, which shows a negative correlation with the SMB (Figure 1e), has changed to a normal positive lag time of 44 days with respect to the local snowfall rate (Figure 2c). The better correlation with the local snowfall rate for station NUUK possibly comes from its high urban construction and less ice sheet coverage. It is also possible that coastal water table or other oceanic variables may explain the variations of *dv/v*, since station NUUK is very close to the coastline. Table 1

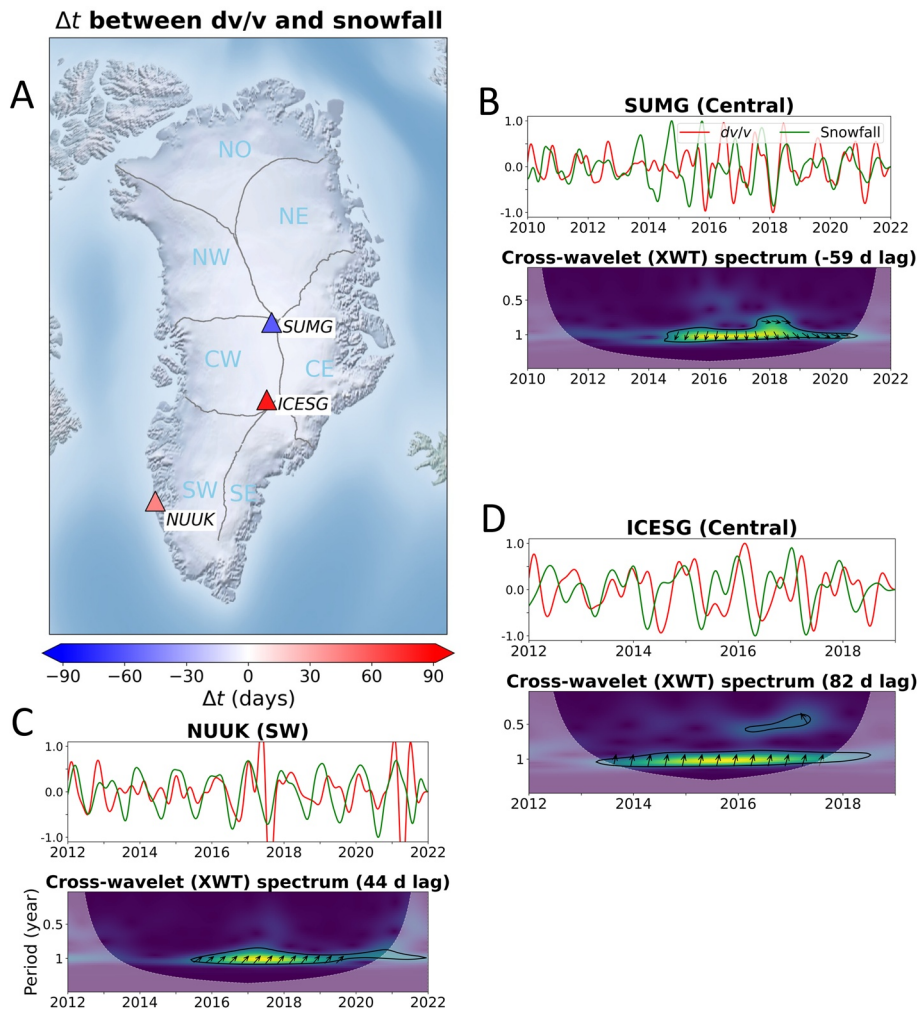

Figure 2. Correlations between *dv/v* with snowfall rates for stations SUMG, ICESG, and NUUK. We use the same method to perform correlation between *dv/v* (red) and local snowfall rate (green) (Hersbach et al., 2018). The snowfall rate data has been standardized and normalized. Other settings are the same as Figure 1.

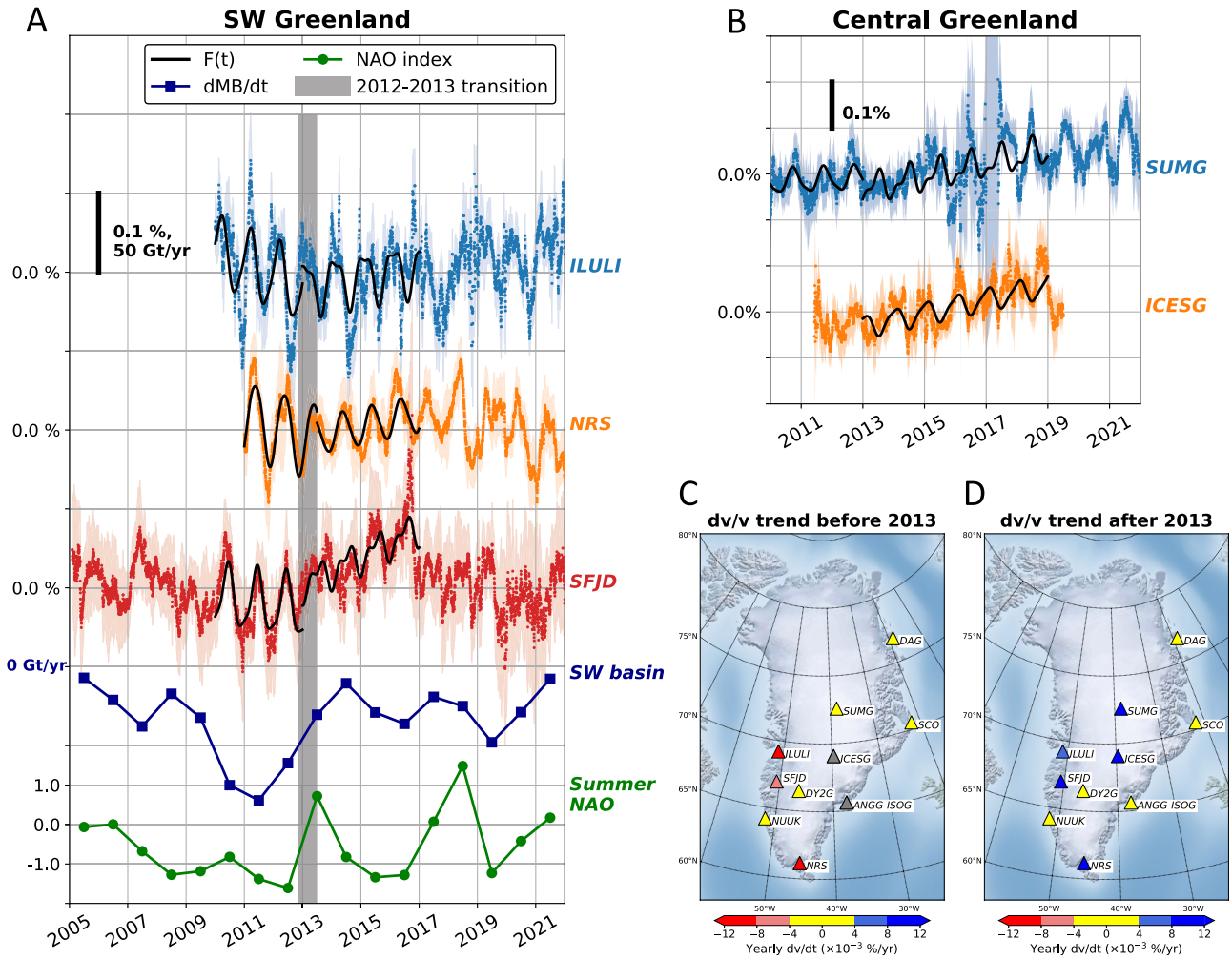

Figure 3. Long-term trend of *dv/v* in the SW and central Greenland over the past two decades. Panel (a) shows the *dv/v* of stations ILULI, NRS and SFJD in the SW Greenland. The fitted errors ($\pm\sigma$, see Text S1 in Supporting Information S1) are shaded. The extreme "2012–2013 warm-cold transition" (The IMBIE Team, 2020) is denoted by the vertical gray bar. We separately fit the *dv/v* variations before and after 2013 by using $F(t)$ in Equation 2 (black curves). The SW annual mass change rate (dM/dt) and summer NAO index are represented by dark blue and green curves, respectively. Panel (b) shows the *dv/v* variations for stations SUMG and ICESG in the central Greenland. Panels (c and d) show the distribution of stations, which are color-coded by their fitted dv/dt (x_5 in Equation 2). Note the increase trend for some SW and central stations after 2013. Gray triangles represent the stations with absence of records.

also summarizes the lag times of *dv/v* with respect to the snowfall rates (with CV values) for these three stations in Greenland.

3.3. Long-Term Trend of *dv/v* With Respect to the Ice Mass Change Rate (*dM/dt*)

It has been widely noted that the GrIS encounters extreme warm summers in 2010–2012 that have induced severe mass loss, while the mass loss abruptly slows down due to the cold summer of 2013 (Bevis et al., 2019; Harig & Simons, 2016; Khazendar et al., 2019; The IMBIE Team, 2020). In Figure 3a, we show *dv/v* time series for stations SFJD, NRS and ILULI in the SW Greenland. Their *dv/v* present indicative turning around early 2013, which possibly correlates with the "2012–2013 warm-cold transition." To better visualize the trends of *dv/v*, we use the following equation to fit the *dv/v* time series:

$$F(t) = x_1 \cos\left(\frac{2\pi(t - x_2)}{365}\right) + x_3 \cos\left(\frac{2\pi(t - x_4)}{182.5}\right) + x_5 t + x_6, \quad (2)$$

where t denotes the time with unit in day. The two cosine terms are used to fit the seasonal fluctuation, while the final regression term $x_5 t + x_6$ is used to represent the linear trend of *dv/v*. Parameters x_1 to x_6 are estimated

Table 2
Yearly Change Rate (dv/dt) of dv/v for Stations in the SW and Central Greenland

Stations	*dv/dt* before 2013 ($\times 10^{-3}$%/yr)	*dv/dt* after 2013 ($\times 10^{-3}$%/yr)	Region
ILULI	-16.2 ± 2.8	6.3 ± 1.4	CW
SFJD	-5.0 ± 2.0	17.8 ± 1.1	SW
NRS	-11.8 ± 2.0	8.2 ± 0.9	SW
SUMG	2.9 ± 1.3	14.0 ± 1.0	Central
ICESG	N/A	14.7 ± 1.2	Central

Note. ±: 95% confidence interval.

by using the nonlinear least-squares regression. We use $F(t)$ to separately fit *dv/v* before and after January of 2013 (black curves in Figure 3a). All these three stations involve the evident negative-positive yearly change rates (*dv/dt*) before and after 2013 (with $|x_5| > 4 \times 10^{-3}$ in Table 2).

In correlation with our *dv/v*, we calculate the annual ice mass change rates (*dM/dt*, i.e., the first derivative of the absolute mass change time series) for different regions of Greenland (Figure S8 in Supporting Information S1). Here, we calculate the annual *dM/dt* by using a 3-year moving window along the time series of the mass change, which is the same procedure as The IMBIE Team (2020)'s analysis. Figure 3a and Figure S8 in Supporting Information S1 show that the *dM/dt* of the SW Greenland has the strongest change during 2010–2013, with a peak loss rate of −84 Gt/yr in 2011. Furthermore, we present the summertime (average of June, July and August) North Atlantic Oscillation (NAO) index in Figure 3a, which is based on differences between the subtropical sea-level high pressure and the subpolar low pressure (National Oceanic and Atmospheric Administration, 2022). Strong negative NAO phases indicate above-normal temperatures in Greenland, and vice versa. There are six successive negative summer NAO indexes before 2012 and an abrupt change (with a ΔNAO of +2.3) to positive in 2013, which indicates that Greenland has gone through extreme warm summers until 2012, then entered an abnormal cold summer in 2013. Therefore, the consistent turning trends of *dv/v*, *dM/dt* and NAO index shown in Figure 3a may suggest that the decrease-increase trend of *dv/v* in the SW Greenland is related to the "2012–2013 warm-cold transition."

In addition, we find a similar turning in the *dv/v* for station SUMG in the central Greenland (Figure 3b). We also see a single increase trend in the *dv/v* for station ICESG due to its incomplete records before 2012. For another SW station NUUK, the absence of similar long-term trend (Figure S9a in Supporting Information S1) probably comes from its limited data coverage and better correlation with the snowfall rate instead of SMB. From stations in other regions of Greenland, we just observe relatively weak long-term trends and small values of *dv/dt* (Figure S9d in Supporting Information S1), which suggest their weak long term mass change rates over the study period. To better visualize the spatial change of the *dv/v* trend, the stations are color-coded by their *dv/dt* before and after the transition period in Figures 3c and 3d, respectively.

Here, we just fit the *dv/v* to the end of 2016. The *dv/v* in the SW Greenland also shows another sharp drop from 2018 to 2019, especially for stations SFJD and NRS (Figure 3a). This observation agrees with previous studies that the GrIS has experienced another extreme mass loss in the summer of 2019 (Velicogna et al., 2020), with ΔNAO of −2.7 from 2018 to 2019 (Figure 3a).

4. Discussion

Mordret et al. (2016) measured *dv/v* between station pairs in the SW/W Greenland, and found *dv/v* has 2–3 months lag with respect to the GrIS mass change estimated from the GRACE measurements. In this study, we observe stable, continuous and positive lag times of *dv/v* for most stations with respect to regional/local surface mass changes (Table 1), which is in good agreement with observations from Mordret et al. (2016). For station SUMG, we find an abnormal negative lag time (Figure 2b). This poor correlation probably results from complex local surface mass variation that may bias our measurements. Another possible explanation is that station SUMG is located on a very thick icesheet, and *dv/v* is less sensitive to deeper processes (see different behaviors of sensitivity kernels in shallower ice layers shown in Figure S5 in Supporting Information S1). For other stations, we note that the lag times of *dv/v* vary from location to location, especially for stations DY2G and ICESG with large lags of 84 and 82 days, respectively (Table 1). Therefore, in this study, we attempt to explore the implications and causes of various *dv/v* lag times at different regions.

Previous studies have proposed different processes to explain active crustal deformation, such as poroelastic (pore pressure diffusion) and viscoelastic (viscous flow inside the curst-mantle system) processes (Segall, 2010). Mordret et al. (2016) investigated these two end-member models, and concluded that the poroelastic model is probably more appropriate to explain the seasonal variation and lag time of *dv/v* due to Greenland's regional geological characteristics (fluids and presence of till layers). This argument comes from the modification of

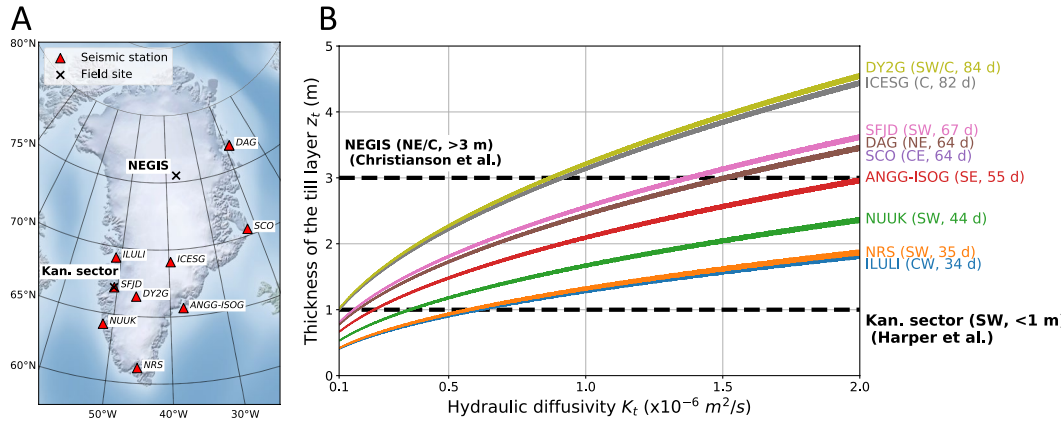

Figure 4. Exploring relation between the *dv*/*v* lag times and the subglacial till layer. Panel (a) shows two field measurements for regional till layer thickness. The Kan. sector represents 32 boreholes near the Kangerlussuaq sector in the SW Greenland (Harper et al., 2017). The NEGIS represents a combined measurement across the central portion of the NE Greenland (Christianson et al., 2014). In Panel (b), each curve represents grid search misfit values less than 0.5 with the combinations of optimal z_t and K_t for each station. Station codes, regions and observed *dv*/*v* lag times (in Table 1) are labeled. Two black dashed lines denote two field measurements of till layers in Panel (a). More details about the parameters can be found in Text S4 in Supporting Information S1.

Tsai (2011), and includes a nonlinear relation between seismic wave speeds changes and pore pressure variations due to surface mass loading/unloading. Based on this model, the lag time of *dv*/*v* (Δt) against the surface pressure can be attributed to the hydraulic properties of incompetent layer and pore pressure diffusion within the bedrock, which can be expressed as (Mordret et al., 2016):

$$\Delta t = \frac{z_t}{\sqrt{2\omega K_t}} + \frac{\cot^{-1}\left(\frac{K_c k^2}{\omega}\right)}{2\omega}, \tag{3}$$

where z_t and K_t are the thickness and hydraulic diffusivity of the incompetent layer, which can be considered as deformable subglacial till layer that exists between iceberg and bedrock in glacial areas (Iverson et al., 1997; Truffer et al., 2000). K_c is the hydraulic diffusivity of the crust, ω and k are the angular frequency and wavenumber of the surface pressure field. The subglacial till layer is the key to understand ice flow and meltwater inputs (Harper et al., 2017), however, direct observations under ice sheets are always challenging. Following Equation 3, we attempt to estimate z_t and K_t by using measured Δt through a grid search (more details about the method and parameters can be found in Text S4 in Supporting Information S1). In Figure 4b, we compare the misfit curves for all stations with different Δt. It is notable that stations DY2G and ICESG, which have larger Δt, are separated from other stations. Coincidentally, these two stations are located in the central region and far away from the ice-ocean boundaries (Figure 4a). Tsai (2011) has conducted a synthetic test and suggested that the thickness of the incompetent layer (z_t) tends to predominantly control the lag time of *dv*/*v* (Δt). Moreover, there are 32 borehole measurements in the Kangerlussuaq sector (with a maximum 30 km separation and <10 km to station SFJD in Figure 4a) in the SW Greenland, which demonstrate that their sediments over bed is <1 m thick (Figure 4b), even absence for some locations (Harper et al., 2017). While, another field investigation has been taken across the central portion of the NE Greenland (NEGIS in Figure 4a), by using radio-echo sounding, GPS and active-source seismic techniques (Christianson et al., 2014). In contrast, their results demonstrate that a dilatant subglacial till layer (at least 3 m thick, see Figure 4b) spreads over a large portion of the central NE Greenland (Christianson et al., 2014). These two field measurements provide us additional references for our speculation that the larger Δt for stations DY2G and ICESG may come from thicker subglacial till layers in the central Greenland. While, other stations near the ice-ocean boundaries with smaller Δt may indicate weak underlying till due to recent deglaciation and/or variable rates of erosion (Harper et al., 2017). We also test Δt of measured *dv*/*v* by using different windows (Figure S4 in Supporting Information S1). For each station, the measured Δt from different windows are basic consistent with each other (Figure S4f in Supporting Information S1). We notice some single early or late windows can lead to biased measurements with large CV values, which is possibly due to different phase types

or higher noise level. Thus, our current window can largely mitigate single window discrepancies and provide reliable Δt measurements. Here, our interpretation of varied Δt is mainly based on the proposed poroelastic model (Mordret et al., 2016), which is just one possible explanation for our observations at the current stage due to our limited knowledge on local glaciological configuration. We certainly cannot exclude other physical processes that may lead to the seasonal variation of dv/v, such as the changes of subglacial channels or cavities and noise source distribution changes.

Another goal of this study is to explore long-term trends of the dv/v. Mordret et al. (2016) have mentioned that the seismic noise correlation technique may not be sensitive to the long-term trends of ice mass loading. However, our results suggest that this seismic-based technique still likely has potential to monitor the long-term trend of the GrIS, since dv/v presents consistent trend with the first derivative of the ice mass change (dM/dt) during the "2012–2013 warm-cold transition," especially in the SW Greenland. The SE Greenland is another region that is probably affected by this abnormal transition, but there is no corresponding trend in dv/v for station pair AGNN-ISOG. Besides the incomplete data records, another possible reason could be the existence of perennial firn aquifer (PFA), which is a liquid water reservoir that persists throughout the wintertime in the SE Greenland (Forster et al., 2014). If this is the case, the measured mass loss by the regional climate models will be overestimated due to the additional meltwater storage of PFA during warm summers (2010–2012). As for two central stations SUMG and ICESG, Toyokuni et al. (2018) performed cross-correlation for this station pair, and obtained a similar increased trend of dv/v from 2011 to 2015. We agree with their analysis that the increase probably comes from the snowstatic pressure accumulation. However, we suggest that the sudden increase trend of dv/v for station SUMG after 2013 is possibly related to the cold transition, which has not been noted by Toyokuni et al. (2018). With lacking of reliable physical mechanisms, we claim that the analysis of dv/v long-term trend is mainly based on our observation of consistency with the mass change rate.

5. Conclusion

We apply a cross-component auto-correlation technique on continuous seismic records from 11 stations in different regions of Greenland to measure relative seismic velocity variation (dv/v) for each individual station. Our measured dv/v have strong seasonal fluctuation, and have indicative long-term trends in some locations. We investigate the correlation between dv/v with ice mass changes in different regions, and observe that the seasonal fluctuation of dv/v has overall less than 3 months lag with respect to the surface ice mass change or local snowfall rates for most stations. The lag times of dv/v may provide constraints for the thickness of subglacial till layers, and a larger dv/v lag time may indicate a thicker till layer, such as in the central Greenland. In the SW Greenland, the long-term trends of dv/v include an abrupt turning at 2013, which may result from the mass change rate due to the "2012–2013 warm-cold transition," However, we cannot exclude other possibilities that may influence dv/v measurements, such as changes of subglacial channels, cavities and noise source distribution. Our observations demonstrate the potential of using seismic noise auto-correlations to monitor seasonal fluctuation and long-term change of the GrIS.

Data Availability Statement

Continuous seismic records are provided by the Incorporated Research Institutions for Seismology, and downloaded by using the BREQ FAST request tool (http://ds.iris.edu/ds/nodes/dmc/forms/breqfast-request/). Seismic noise correlations are calculated by using the MSNoise package (Lecocq et al., 2014). The data set of the Greenland Ice Sheet mass balance comes from the Programme for Monitoring of the Greenland Ice Sheet, Denmark (Mankoff et al., 2021). The datasets of snowfall rate and 2-m-high level air temperature are collected from the ERA5 program (Hersbach et al., 2018). The wavelet spectral analysis is performed by using PyCWT package (https://github.com/regeirk/pycwt). The North Atlantic Oscillation index comes from the National Oceanic and Atmospheric Administration (https://www.ncei.noaa.gov/access/monitoring/nao/). All figures are plotted by using Matplotlib 3.3.0 (Hunter, 2007).

Acknowledgments
The authors acknowledge insightful and careful reviews by Dr. Victor Tsai and another anonymous reviewer. The authors thank productive discussions with Dr. Christopher Harig on Greenland Ice Sheet monitoring and GRACE measurements. This research is supported by U.S. National Science Foundation Grant EAR2042098.

References

Bevis, M., Harig, C., Khan, S. A., Brown, A., Simons, F. J., Willis, M., et al. (2019). Accelerating changes in ice mass within Greenland, and the ice sheet's sensitivity to atmospheric forcing. *Proceedings of the National Academy of Sciences*, *116*(6), 1934–1939. https://doi.org/10.1073/pnas.1806562116

Brenguier, F., Shapiro, N., Campillo, M., Ferrazzini, v., Duputel, Z., Coutant, O., & Nercessian, A. (2008). Toward forecasting volcanic eruption using seismic noise. *Nature Geoscience*, *1*(2), 126–130. https://doi.org/10.1038/ngeo104

Campillo, M., & Paul, A. (2003). Long-range correlations in the diffuse seismic coda. *Science*, *299*(5606), 547–549. https://doi.org/10.1126/science.1078551

Chen, J. L., Wilson, C. R., & Tapley, B. D. (2006). Satellite gravity measurements confirm accelerated melting of Greenland Ice Sheet. *Science*, *313*(5795), 1958–1960. https://doi.org/10.1126/science.1129007

Christianson, K., Peters, L. E., Alley, R. B., Anandakrishnan, S., Jacobel, R. W., Riverman, K. L., et al. (2014). Dilatant till facilitates ice-stream flow in northeast Greenland. *Earth and Planetary Science Letters*, *401*, 57–69. https://doi.org/10.1016/j.epsl.2014.05.060

Clarke, D., Zaccarelli, L., Shapiro, N. M., & Brenguier, F. (2011). Assessment of resolution and accuracy of the Moving Window Cross Spectral technique for monitoring crustal temporal variations using ambient seismic noise. *Geophysical Journal International*, *186*(2), 867–882. https://doi.org/10.1111/j.1365-246X.2011.05074.x

Forster, R., Box, J., Van den Broeke, M., Miege, C., Burgess, E., van angelen, J., et al. (2014). Extensive liquid meltwater storage in firn within the Greenland Ice Sheet. *Nature Geoscience*, *7*(2), 95–98. https://doi.org/10.1038/ngeo2043

Harig, C., & Simons, F. J. (2012). Mapping Greenland's mass loss in space and time. *Proceedings of the National Academy of Sciences of the United States of America*, *109*(49), 19934–19937. https://doi.org/10.1073/pnas.1206785109

Harig, C., & Simons, F. J. (2016). Ice mass loss in Greenland, the Gulf of Alaska, and the Canadian Archipelago: Seasonal cycles and decadal trends. *Geophysical Research Letters*, *43*(7), 3150–3159. https://doi.org/10.1002/2016GL067759

Harper, J. T., Humphrey, N. F., Meierbachtol, T. W., Graly, J. A., & Fischer, U. H. (2017). Borehole measurements indicate hard bed conditions, kangerlussuaq sector, western Greenland Ice Sheet. *Journal of Geophysical Research: Earth Surface*, *122*(9), 1605–1618. https://doi.org/10.1002/2017JF004201

Helm, V., Humbert, A., & Miller, H. (2014). Elevation and elevation change of Greenland and Antarctica derived from CryoSat-2. *The Cryosphere*, *8*(4), 1539–1559. https://doi.org/10.5194/tc-8-1539-2014

Hersbach, H., Bell, B., Berrisford, P., Biavati, G., Horányi, A., Muñoz Sabater, J., et al. (2018). ERA5 hourly data on single levels from 1959 to present. *Copernicus Climate Change Service (C3S) Climate Data Store (CDS)*. https://doi.org/10.24381/cds.adbb2d47

Hunter, J. D. (2007). Matplotlib: A 2D graphics environment. *Computing in Science & Engineering*, *9*(3), 90–95. https://doi.org/10.1109/MCSE.2007.55

Iverson, N. R., Baker, R. W., & Hooyer, T. S. (1997). A ring-shear device for the study of till deformation: Tests on tills with contrasting clay contents. *Quaternary Science Reviews*, *16*(9), 1057–1066. https://doi.org/10.1016/S0277-3791(97)00036-X

Joughin, I., Das, S. B., King, M. A., Smith, B. E., Howat, I. M., & Moon, T. (2008). Seasonal speedup along the western flank of the Greenland Ice Sheet. *Science*, *320*(5877), 781–783. https://doi.org/10.1126/science.1153288

Khan, S. A., Kjær, K. H., Bevis, M. G., Bamber, J. L., Wahr, J. M., Kjeldsen, K. K., et al. (2014). Sustained mass loss of the northeast Greenland Ice Sheet triggered by regional warming. *Nature Climate Change*, *4*, 292–299. https://doi.org/10.1038/nclimate2161

Khazendar, A., Fenty, I., Carroll, D., Gardner, A., Lee, C., Fukumori, I., et al. (2019). Interruption of two decades of Jakobshavn Isbrae acceleration and thinning as regional ocean cools. *Nature Geoscience*, *12*(4), 1–7. https://doi.org/10.1038/s41561-019-0329-3

Lecocq, T., Caudron, C., & Brenguier, F. (2014). MSNoise, a Python package for monitoring seismic velocity changes using ambient seismic noise. *Seismological Research Letters*, *85*(3), 715–726. https://doi.org/10.1785/0220130073

Luthcke, S. B., Rowlands, D. D., Lemoine, F. G., Klosko, S. M., Chinn, D., & McCarthy, J. J. (2006). Monthly spherical harmonic gravity field solutions determined from GRACE inter-satellite range-rate data alone. *Geophysical Research Letters*, *33*(2), L02402. https://doi.org/10.1029/2005GL024846

Machguth, H., Macferrin, M., van As, D., Box, J., Charalampidis, C., Colgan, W., et al. (2016). Greenland meltwater storage in firn limited by near-surface ice formation. *Nature Climate Change*, *6*(4), 390–393. https://doi.org/10.1038/nclimate2899

Mankoff, K. D., Fettweis, X., Langen, P. L., Stendel, M., Kjeldsen, K. K., Karlsson, N. B., et al. (2021). Greenland Ice Sheet mass balance from 1840 through next week. *Earth System Science Data*, *13*(10), 5001–5025. https://doi.org/10.5194/essd-13-5001-2021

Mao, S., Mordret, A., Campillo, M., Fang, H., & van der Hilst, R. D. (2019). On the measurement of seismic traveltime changes in the time–frequency domain with wavelet cross-spectrum analysis. *Geophysical Journal International*, *221*(1), 550–568. https://doi.org/10.1093/gji/ggz495

Mordret, A., Jolly, A., Duputel, Z., & Fournier, N. (2010). Monitoring of phreatic eruptions using interferometry on retrieved cross-correlation function from ambient seismic noise: Results from Mt. Ruapehu, New Zealand. *Journal of Volcanology and Geothermal Research*, *191*(1), 46–59. https://doi.org/10.1016/j.jvolgeores.2010.01.010

Mordret, A., Mikesell, T. D., Harig, C., Lipovsky, B. P., & Prieto, G. A. (2016). Monitoring southwest Greenland's ice sheet melt with ambient seismic noise. *Science Advances*, *2*(5), e1501538. https://doi.org/10.1126/sciadv.1501538

Morlighem, M., Williams, C. N., Rignot, E., An, L., Arndt, J. E., Bamber, J. L., et al. (2017). BedMachine v3: Complete bed topography and ocean bathymetry mapping of Greenland from multibeam echo sounding combined with mass conservation. *Geophysical Research Letters*, *44*(21), 11051–11061. https://doi.org/10.1002/2017GL074954

Mouginot, J., & Rignot, E. (2019). Glacier catchments/basins for the Greenland Ice Sheet. *Dryad*. https://doi.org/10.7280/D1WT11

Mouginot, J., Rignot, E., Bjørk, A. A., van den Broeke, M., Millan, R., Morlighem, M., et al. (2019). Forty-six years of Greenland Ice Sheet mass balance from 1972 to 2018. *Proceedings of the National Academy of Sciences*, *116*(19), 9239–9244. https://doi.org/10.1073/pnas.1904242116

National Oceanic and Atmospheric Administration. (2022). National centers for environmental information, North Atlantic oscillation (NAO). Retrieved from https://www.ncei.noaa.gov/access/monitoring/nao/

Pacheco, C., & Snieder, R. K. (2005). Time-lapse travel time change of multiply scattered acoustic waves. *Journal of the Acoustical Society of America*, *118*(3), 1300–1310. https://doi.org/10.1121/1.2000827

Pritchard, H., Arthern, R., Vaughan, D., & Edwards, L. (2009). Extensive dynamic thinning on the margins of the Greenland and Antarctic Ice Sheets. *Nature*, *461*(7266), 971–975. https://doi.org/10.1038/nature08471

Programme for Monitoring of the Greenland Ice Sheet. (2022). The Greenland Ice Sheet page. Retrieved from https://promice.org/greenland-ice-sheet

Ramillien, G., Lombard, A., Cazenave, A., Ivins, E., Llubes, M., Remy, F., & Biancale, R. (2006). Interannual variations of the mass balance of the Antarctica and Greenland Ice Sheets from GRACE. *Global and Planetary Change*, *53*(3), 198–208. https://doi.org/10.1016/j.gloplacha.2006.06.003

Richter, T., Sens-Schönfelder, C., Kind, R., & Asch, G. (2014). Comprehensive observation and modeling of earthquake and temperature-related seismic velocity changes in northern Chile with passive image interferometry. *Journal of Geophysical Research: Solid Earth*, *119*(6), 4747–4765. https://doi.org/10.1002/2013JB010695

Rignot, E., Box, J. E., Burgess, E., & Hanna, E. (2008). Mass balance of the Greenland Ice Sheet from 1958 to 2007. *Geophysical Research Letters*, *35*(20), L20502. https://doi.org/10.1029/2008GL035417

Sandberg Sørensen, L., Simonsen, S. B., Forsberg, R., Khvorostovsky, K., Meister, R., & Engdahl, M. E. (2018). 25 years of elevation changes of the Greenland Ice Sheet from ERS, Envisat, and CryoSat-2 radar altimetry. *Earth and Planetary Science Letters*, *495*, 234–241. https://doi.org/10.1016/j.epsl.2018.05.015

Segall, P. (2010). *Earthquake and volcano deformation* (STU - Student edition ed.). Princeton University Press.

Sens-Schönfelder, C., & Wegler, U. (2006). Passive image interferometry and seasonal variations of seismic velocities at Merapi Volcano, Indonesia. *Geophysical Research Letters*, *33*(21), L21302. https://doi.org/10.1029/2006GL027797

Shepherd, A., Ivins, E. R., Geruo, A., Barletta, V. R., Bentley, M. J., Bettadpur, S., et al. (2012). A reconciled estimate of Ice-Sheet mass balance. *Science*, *338*(6111), 1183–1189. https://doi.org/10.1126/science.1228102

The IMBIE Team. (2020). Mass balance of the Greenland Ice Sheet from 1992 to 2018. *Nature*, *579*(7798), 233–239. https://doi.org/10.1038/s41586-019-1855-2

Torrence, C., & Compo, G. P. (1998). A practical guide to wavelet analysis. *Bulletin of the American Meteorological Society*, *79*(1), 61–78. https://doi.org/10.1175/1520-0477(1998)079⟨0061:APGTWA⟩2.0.CO;2

Toyokuni, G., Takenaka, H., Takagi, R., Kanao, M., Tsuboi, S., Tono, Y., et al. (2018). Changes in Greenland ice bed conditions inferred from seismology. *Physics of the Earth and Planetary Interiors*, *277*, 81–98. https://doi.org/10.1016/j.pepi.2017.10.010

Truffer, M., Harrison, W. D., & Echelmeyer, K. A. (2000). Glacier motion dominated by processes deep in underlying till. *Journal of Glaciology*, *46*(153), 213–221. https://doi.org/10.3189/172756500781832909

Trusel, L. D., Das, S. B., Osman, M. B., Evans, M. J., Smith, B. E., Fettweis, X., et al. (2018). Nonlinear rise in Greenland runoff in response to post-industrial Arctic warming. *Nature*, *564*(7734), 104–108. https://doi.org/10.1038/s41586-018-0752-4

Tsai, V. C. (2011). A model for seasonal changes in GPS positions and seismic wave speeds due to thermoelastic and hydrologic variations. *Journal of Geophysical Research*, *116*(B4), B04404. https://doi.org/10.1029/2010JB008156

Velicogna, I., Mohajerani, Y., Geruo, A., Landerer, F., Mouginot, J., Noel, B., et al. (2020). Continuity of ice sheet mass loss in Greenland and Antarctica from the GRACE and GRACE follow-on missions. *Geophysical Research Letters*, *47*(8), e2020GL087291. https://doi.org/10.1029/2020GL087291

Wegler, U., & Sens-Schönfelder, C. (2007). Fault zone monitoring with passive image interferometry. *Geophysical Journal International*, *168*(3), 1029–1033. https://doi.org/10.1111/j.1365-246X.2006.03284.x

Zheng, L., Cheng, X., Shang, X., Chen, Z., Liang, Q., & Wang, K. (2022). Greenland Ice Sheet daily surface melt flux observed from space. *Geophysical Research Letters*, *49*(6), e2021GL096690. https://doi.org/10.1029/2021GL096690

Zwally, H. J., Giovinetto, M. B., Li, J., Cornejo, H. G., Beckley, M. A., Brenner, A. C., et al. (2005). Mass changes of the Greenland and Antarctic ice sheets and shelves and contributions to sea-level rise: 1992–2002. *Journal of Glaciology*, *51*(175), 509–527. https://doi.org/10.3189/172756505781829007